JOURNAL OF MATERIALS SCIENCE 30 (1995) 1037–1045

Processing of microcellular SiC foams

Part II *Ceramic foam production*

T. J. FITZGERALD, V. J. MICHAUD, A. MORTENSEN
Department of Materials Science and Engineering, Massachusetts Institute of Technology, MA, USA

A replication process for producing fine open-celled ceramic foam from preceramic polymers is presented and analysed. In this process,a porous sodium chloride compact formed by sintering was first infiltrated with polycarbosilane. After dissolution of the salt, the resulting polymer foam was cured by oxidation in air and pyrolysed to form a silicon carbide foam. The curing stage is the most critical step, and was investigated using a series of controlled curing experiments and finite-difference modelling of heat transfer during curing. Good agreement has been found between theory and experiment. The model was then used to investigate the limits of the process and to provide stategies for successful curing of the foams without melting or cracking.

1. Introduction

We present and analyse a process for producing fine open-celled ceramic foams starting with a preceramic polymer. The rationale for this investigation was presented in Part I [1] in which the curing kinetics of commercially available polycarbosilane in air were measured. In Part II we focus on the foam process, basing our analysis on result from Part I.

Processes which have been developed for the fabrication of fine ceramic foams have been described by several authors [2–6]. These include: (i) the slurry process, whereby a polymer foam is coated with a ceramic slurry which is subsequently sintered while the polymer is burned off; (ii) chemical vapour deposition of a ceramic on a thin carbon foam; (iii) aerogel process; and (iv) co-pressing and binding of ceramic fibres. Each process has its advantages and drawbacks; for example, the slurry process is economical, but generally produces comparatively weak and coarse-celled ceramic foams.

The process presented here starts with the production of a polymer foam via the replication process, whereby the polymer is injected into a porous substrate which is later removed. Replication has been used in the production of several cellular solids, including microcellular carbon foam by conversion of a polymer precursor within the porous substrate [4, 7–9]. Advantages of replication foam processing include extensive control of foam architecture, with the possibility for the production of fine and regularly sized cells having fully dense struts, unlike foams derived by coating a substrate which is later removed. The silicon carbide foams presented here have, to the best of our knowledge, cell sizes about an order of magnitude finer than that in commercially available foams of SiC, which were produced by alternative processes explored to date, such as chemical vapour deposition [10].

Because the viscosity of molten polycarbosilane is relatively high and capillary forces are insufficient to drive the polymer rapidly into the salt, the polycarbosilane is driven into the salt preform under applied pressure. Following infiltration, the sample is placed in water and the salt network is leached away. This results in an open-celled polycarbosilane foam which is then dried. Once dry, the foam is cured, so that it is transformed from a thermoplastic polymer to a thermoset, which will not melt during subsequent pyrolysis to form the ceramic. In this work, the conventional oxidative curing process is used, whereby the polymer is cross-linked by reaction with oxygen, which is introduced into the polycarbosilane foam by heating in air (see Part I). As will be shown below, this step of the process is the most critical. After curing, the cured polycarbosilane is converted to silicon carbide by pyrolysis.

In Part II we present first the foam production technique in detail, together with observations and measurements relevant to the process. A quantitative thermal analysis is then made of the foam curing step, to show the physical origin of observed process limitations. Theoretical predictions are then compared with experiment, and discussed.

2. Experimental procedure and results

2.1 Ceramic foam production process

Fine-grain sodium chloride, TCP-66™ purchased from Akzo (Clarks Summit, PA), was used to make the sintered salt compacts. Such salt is convenient to use because it is pre-ground, inexpensive and easy to work with; however, it is somewhat impure, because it contains 1.5 wt of tricalcium phosphate which acts as an anti-caking agent.

The as-received sodium chloride was sifted according to grain size. Approximately 100 ml as-received salt was poured on to a stack of brass and stainless steel sieves 8 in diameter, and agitated for approximately 2 h using a Tyler (Cleveland, OH) Rotap™ sieve

0022–2461

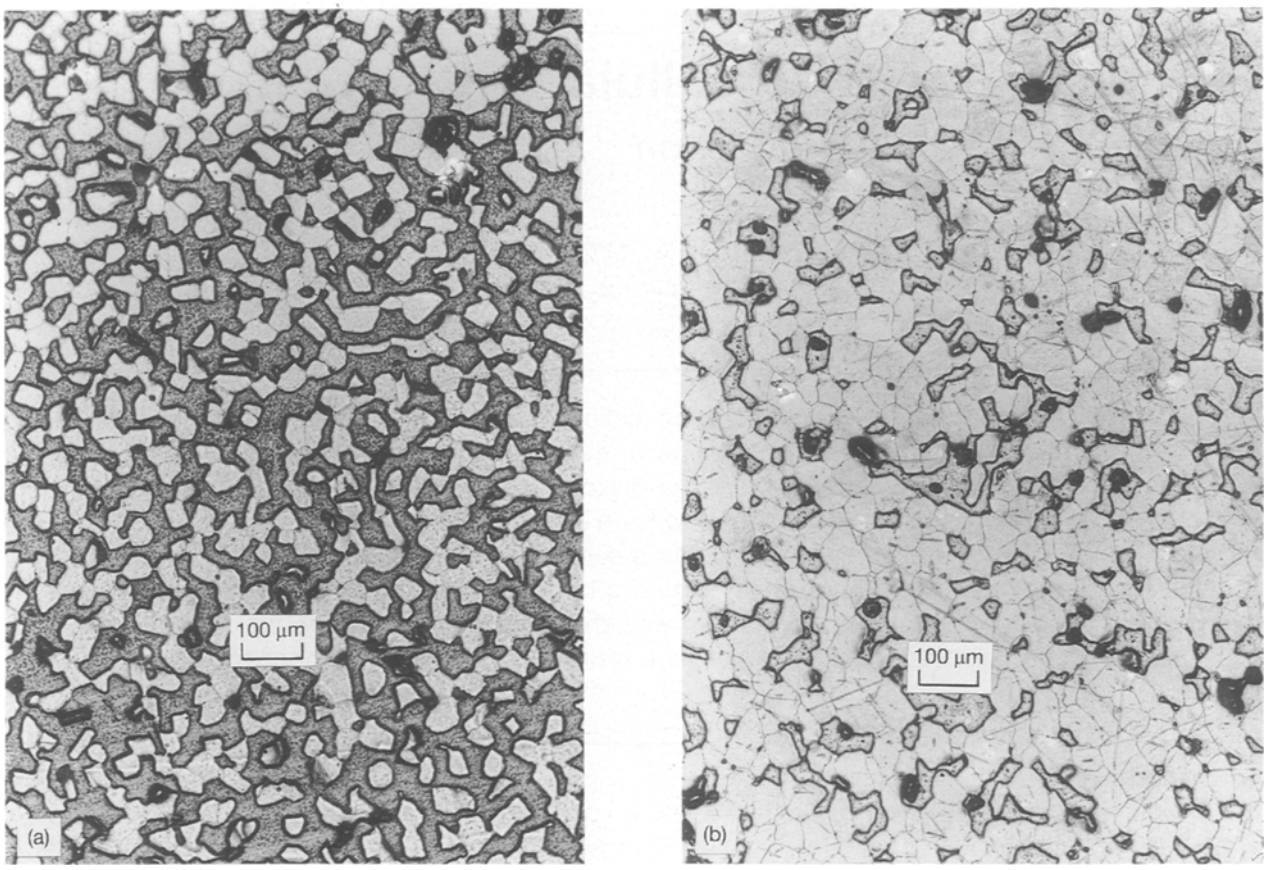

Figure 1 Representative structures of sintered salt compacts. The light phase is salt, and the dark phase is epoxy (used for metallography). (a) 45–53 μm salt sintered 4 days at 795 °C; (b) 53–75 μm salt compressed to 10 000 p.s.i. (10^3 p.s.i = 6.89 N mm^{-2}), and then sintered 4 days at 795 °C.

shaker. The mesh sizes used were 140, 170, 270, and 325 (which correspond to grain sizes of 106, 90, 75, 53 and 45 μm, respectively). Sieves finer than 325 mesh were not used because the salt had difficulty passing through such screens. This sifting method worked well for sodium chloride using tricalcium phosphate as a anti-caking agent. Comparatively, sifting salt containing glycerine as an anti-caking agent was slow and generally ineffective.

The sifted salt was then placed in quartz tubes lined with UCAR (Cleveland, OH) Grafoil™ graphite foil. Plugs of Carborundum (Niagara Falls, NY) Fiberfrax™ alumina–silica insulation, also lined with Grafoil™, were used to seal the ends of the tube. Grafoil™ was used to prevent the salt from sticking to the quartz during sintering. The tube was tapped by hand to help the salt settle. When a higher packing density was desired, the salt was compressed in a Grafoil™ lined steel die using a 20 ton press.

Sodium chloride compacts were then placed in a Lindberg (Chicago, IL) 55346 three-zone tube furnace under a flowing argon atmosphere, and sintered at 795 °C for periods ranging from 1–6 days depending on the salt grain size. Sintering cycles for the salt compacts were determined largely by trial and error, with a goal to produce salt compacts having a smooth pore surface and a volume fraction of about 50%. Sintering conditions used are given in Table I.

Sample preparation for examination of the salt compacts in reflective light microscopy was performed after vacuum infiltration with low-viscosity epoxy. Following setting of the epoxy, samples were ground flat with 600 grit silicon carbide paper and then polished on a nylon polishing cloth using a liberal amount of 9, 3 and 1 μm diamond paste and no lubricating fluid. Between polishing steps, samples were cleaned in an ultrasonic bath of pentane. Finally, to enhance contrast, the salt phase was lightly etched by placing samples in an ultrasonic bath of ethanol for approximately 15 s. The microstructures of two sintered salt compacts are shown in Fig. 1.

In the next stage of the process, porous salt compacts were infiltrated with molten polycarbosilane. In preliminary work, infiltration was achieved by simply heating polycarbosilane and sintered salt compacts together in a tube furnace containing a neutral atmosphere. However, the rate of infiltration was exceedingly low, and air and effluent gases often became trapped in the sample cores. Hence, pressure infiltration was used.

Pressure infiltration was conducted using the apparatus described by Isaacs *et al.* [11]: a salt compact was placed in the bottom of a closed-end Pyrex tube

TABLE I Sintering conditions for NaCl compacts

Grain size (μm)	Temperature (°C)	Sintering time (days)
< 45	795	1
45–53	795	4
53–75	795	4
75–90	795	6

and the tube was filled with an equivalent volume of polycarbosilane. The Pyrex tube was then placed in a stainless steel holder, and the entire unit was lowered into a pressure vessel. Next, the vessel was sealed, purged of air, and argon at 1 atm was introduced. Samples were heated to 435 °C at which point argon at 7 MPa was allowed to flow into the vessel, thus forcing molten polycarbosilane into all open pores of the salt compact. Samples were then solidified under pressure. When cool, the sample was dislodged from the Pyrex tube and excess polycarbosilane was removed using a razor blade.

The salt was leached from the samples using water. First, samples were placed in a Pyrex beaker which was then evacuated and sealed. The inlet of the beaker was immersed in distilled water, and the seal was broken. Once the beaker was filled with water, the samples were quickly transferred to a large bath of continuously stirred distilled water. The bath water was changed once a day for approximately 3 weeks (this time was determined from an estimation of the rate of salt diffusion through the polycarbosilane foam). At the end of this period, samples were removed, placed on wire screens, and dried in a convection oven. Samples were dried at 35 °C for 12 h, then at 50 °C for 12 h, and finally at 75 °C for 24 h.

PCS foam was cured from a thermoplastic to a thermoset by direct oxidation at elevated temperatures in a Thermolyne (Dubuque, IA) 9000 series convection oven (model 47335), typically by raising the oven temperature from 100 °C to 190 °C at 0.02 °C min^{-1}. Samples were placed in regions of the convection oven featuring good air circulation in order to minimize heat buildup within the samples.

Finally, samples were pyrolysed in a Lindberg (Chicago, IL) 55346 three-zone tube furnace containing an argon atmosphere. The pyrolysis cycle consisted of a ramp from room temperature to 1100 °C at 0.5 °C min. During pyrolysis, cured polycarbosilane foams were placed on a bed of carbon rollers, which allowed the cylindrical foam samples to shrink freely during pyrolysis, thereby minimizing possible foam cracking, Fig. 2.

The foam production process outlined above allows independent control of microstructural parameters

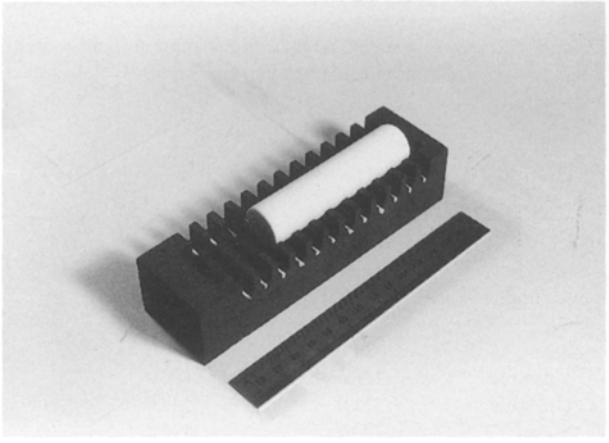

Figure 2 Cured polycarbosilane foam on carbon rollers prior to pyrolysis.

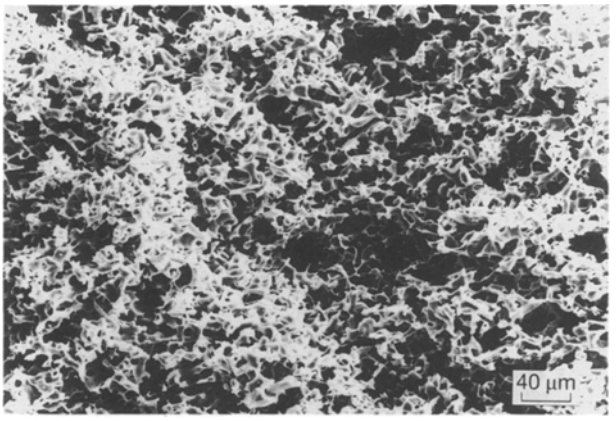

Figure 3 SiC foam fracture surface.

that are normally coupled in conventional foaming processes. For instance, the cell size of the foam can be independently adjusted simply by varying the size of the salt used. The relative density of the foam can be adjusted by packing and sintering the salt to different densities.

A scanning electron micrograph of a typical fracture surface of the resulting SiC foam is seen in Fig.3. Cells are seen to be open and of uniform size. Observation at higher magnification showed that cell struts are dense. Cell sizes down to 10 μm were produced in this manner, which is approximately an order of magnitude smaller than the finest commercially available SiC foams currently produced by chemical vapour infiltration. The internal foam surface is relatively smooth, which stems from vapour mass transport during sintering of salt powder [12, 13].

2.2. Controlled curing experiments

The production of polycarbosilane foam as described was generally straight-forward (provided the uncured polycarbosilane foam was handled with care), with the exception of the curing stage. Depending on curing conditions, white cured polycarbosilane foams of high integrity were produced, or alternatively, partly melted, or cracked and brownish foams were produced. Controlled experiments, in which the sample and ambient temperature were simultaneously recorded during curing, were therefore performed to gain a better understanding of heat generation and transport in the curing process.

The apparatus for these experiments is shown in Fig. 4, and consisted of a cylinder of polycarbosilane foam placed between two cylinders of fibrous ceramic insulation hung in position using thin stainless steel wires. Through one cylinder of insulation, a thin type K thermocouple was strung, which terminated in the centre of the polycarbosilane foam. A second thermocouple was placed approximately 3 cm below the foam to measure the ambient temperature. This assembly was placed in a Thermolyne (Dubuque, IA) 9000 series convection oven equipped with a digital programmable temperature controller. A sheet of aluminium honeycomb was placed below the cylinders to help direct the vertical forced air flow.

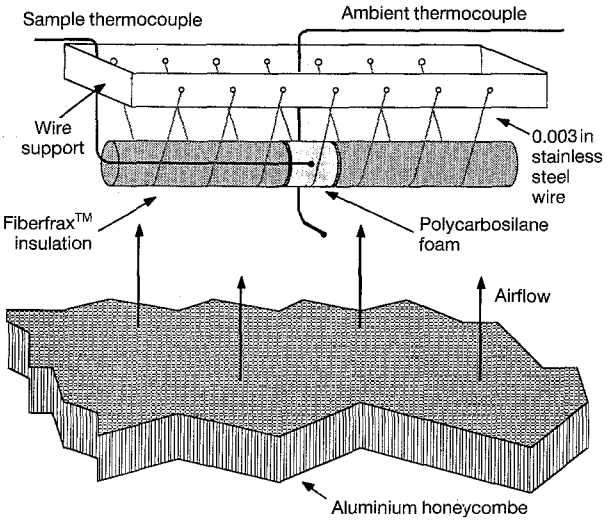

Figure 4 Experimental set-up placed inside the convection oven to monitor the foam curing process.

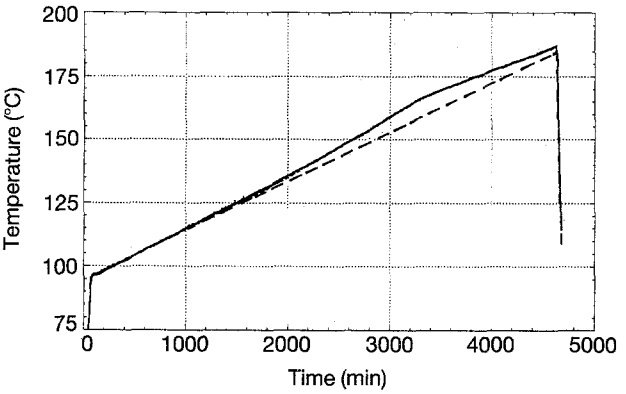

Figure 5 Thermal history of PCS foam sample A, which displayed a moderate exotherm and cured successfully. (——) Sample, (– – –) ambient.

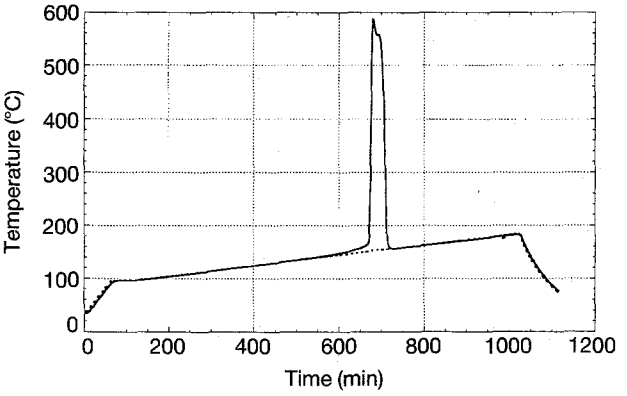

Figure 6 Thermal history of PCS foam sample C, which experienced thermal runaway. (——) Sample, (– – –) ambient.

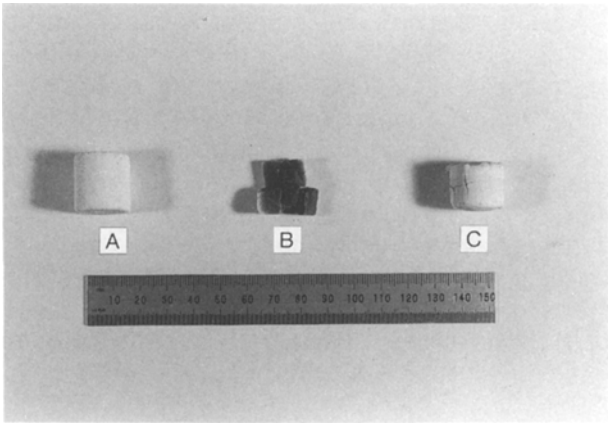

Figure 7 Samples A, B and C after curing. Sample A is successfully cured, sample B shows signs of cracking, and Sample C shows signs of melting.

The signals from the thermocouples were read by two thermocouple indicators which, in turn, were attached to an analogue digital converter for direct data entry into a computer. The thermocouples were calibrated using the melting point of tin at elevated temperatures and a mercury thermometer at room temperature.

Six separate curing experiments were performed using foams of varying diameter. All samples of foam were from the same batch, and had a cell size of approximately 100 μm and a relative density of 0.40. Samples of foam were placed in the same location in the centre of the oven for every run. For each run, the ambient temperature was raised from room temperature to 100 °C at 1 °C min^{-1}, followed by a soak at 100 °C for 1 h. Thereafter, the temperature was raised to 190 °C at the rate given in Table II. For runs A and C the second temperature ramp began at 96.5 °C and ended at 186.5 °C (due to a controller offset error).

A summary of the experimental results is given in Table II, where T_{crit} is defined as the ambient temperature at which either (i) an exotherm peak (Fig. 5) or (ii) a rapidly increasing temperature was detected (Fig. 6; this phenomenon is designated thermal runaway). Samples which cured successfully (A, D and F) displayed a maximum exotherm during the curing cycle and had the same appearance before and after curing. Samples experiencing thermal runaway were defective. Fig. 7 shows samples which failed by thermal runaway: these appeared either red/brown and

TABLE II Summary of curing experiments

	Diameter (cm)	Ramp rate (°C min^{-1})	Curing results (actual)	Curing results (computer model)	T_{crit} (actual) (°C)	T_{crit} (computer model) (°C)
A	2.0	0.02	Stable	Stable	161.0	160.0
B	2.0	0.04	Unstable	Unstable	156.5	160.0
C	2.0	0.10	Unstable	Unstable	151.0	148.0
D	1.27	0.04	Stable	Stable	183.0	172.5
E	1.27	0.10	Unstable	Unstable	182.5	172.5
F	0.76	0.10	Stable	Stable	189.0	187.5

cracked into many pieces (B), or yellow with signs of partial melting (C). The samples which cracked into many pieces showing no signs of melting displayed gradients in colour, becoming progressively lighter towards their radial surface. Similar longitudinal colour gradients were also present along the lateral surfaces of these samples (contacting the ceramic insulation); however, their width was much smaller than along cylindrical walls. This observation, coupled with the structural radial symmetry of the samples away from their ends, indicates that heat transfer between the samples and the ceramic insulators was negligible in comparison to radial heat exchange with the surrounding atmosphere.

To measure the heat-transfer coefficient between the PCS cylinders and the ambient atmosphere during these controlled curing experiments, a cylinder of high-purity copper 2.0 cm diameter, was also placed in place of a foam sample in the apparatus used to monitor foam curing (depicted in Fig. 4). A thin type K thermocouple coated with Omega (Stamford, CT) Omegatherm 201™ high thermal conductivity thermal paste was inserted into a hole drilled to the centre of the copper sample. The ambient temperature in the oven was raised from room temperature to 100 °C and the system was allowed to come to thermal equilibrium. Thereafter, the temperature was raised to 200 °C at 1 °C min^{-1}. The measured difference between the sample and ambient temperatures is given in Fig. 8 and seen to level off at a constant value of 11.4 °C.

Assuming Newtonian heat transfer between the sample and its surroundings, i.e. $Bi = hD/k < 0.1$, where D is the sample diameter, k is the thermal conductivity and h is the heat transfer coefficient, h can be deduced

$$h = \frac{D\rho C_p}{4}\frac{1}{\Delta T}\frac{dT}{dt} \quad (1)$$

where ρ is the copper density, C_p the copper heat capacity, T the copper sample temperature, and ΔT the temperature difference between the ambient atmosphere and the copper. Inserting the values for the density and thermal conductivity of copper yields $h = 25.2\ W\,m^{-2}\,K^{-1}$, in turn yielding $Bi = 0.0013$, consistent with the assumption of Newtonian heat transfer.

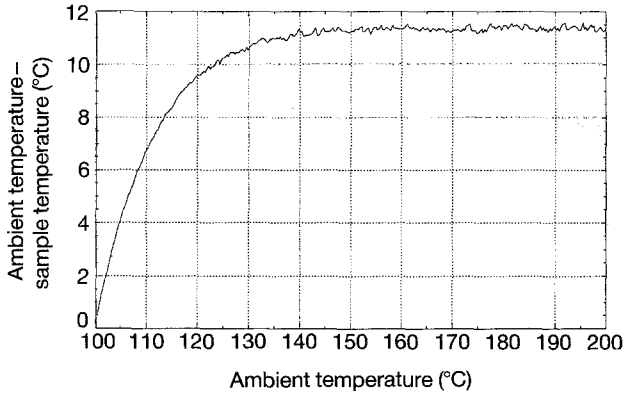

Figure 8 Heat-up curve of a cylinder of copper 2 cm diameter placed in lieu of a sample in the set-up drawn in Fig. 4. Ambient temperature was raised at 1 °C min^{-1}.

3. Theoretical analysis of oxidative foam curing in air

3.1. The computer model

A numerical computer model was developed which simulates the curing behaviour of macroscopic cylinders of PCS foam. The model treats a cylinder of PCS foam placed in a convection oven, in which the ambient temperature is being raised at a constant rate. Both forced and natural convection are assumed. The cylinder is assumed to have infinite length, thus end effects have been neglected.

Heat transfer within the cylindrical foam is governed by Fourier's Law, with an additional term accounting for heat generated by chemical reaction

$$\frac{\partial T}{\partial t} = \frac{k}{\rho C_p}\left(\frac{\partial^2 T}{\partial r^2} + \frac{1}{r}\frac{\partial T}{\partial r}\right) + \frac{\dot{Q}}{\rho C_p} \quad (2)$$

where Q is the rate of heat generation, and r the radius within the cylinder. Heat transfer at the surface of the cylinder is by convection to the surrounding atmosphere, controlled by a heat transfer coefficient, h

$$k\left(\frac{\partial T}{\partial r}\right)_s = h(T_a - T_s) \quad (3)$$

where the subscript s refers to the cylinder surface, and T_a is the ambient temperature. By symmetry, at the centre of the cylinder the temperature gradient is zero.

Q was computed based on empirical equations reported in Part I [1], giving the rate of heat released as a function of local temperature and fraction conversion, α, at that temperature. Use of the equations derived in Part I is made under the assumption that the rate of heat generation is governed by these two parameters only, regardless of prior history of the curing polycarbosilane. This assumption was shown in Part I to agree with data measured on a sample subjected to a non-isothermal curing sequence.

Equation 2 as solved using the Crank–Nicolson finite difference method [14], the cylinder of radius R being divided into equally spaced intervals. Finite-difference equations and computer codes are listed elsewhere [15].

3.2. Evaluation of physical parameters

3.2.1. Foam thermal properties

No values have seemingly been published for the thermal conductivity of polycarbosilane [16]; hence, an estimate of 0.25 $W\,m^{-1}\,°C^{-1}$ is made (the thermal conductivity of most polymers lies within a factor of two of this value [2]). An estimate for the thermal conductivity of the foam is made by multiplying the bulk thermal conductivity by the relative density and an efficiency factor accounting for the foam's tortuosity. Following the work of Schuetz and Glicksman [17], a tortuosity factor of 2/3 is chosen (the value of 2/3 has been shown to be both theoretically and experimentally correct for foams of high density containing a large portion of the polymer mass in the cell

walls [17]). Hence

$$k = 0.167\ V_f (\mathrm{W\,m^{-2}\,^\circ C^{-1}}) \quad (4)$$

where V_f is the relative foam density. Using this value for k, the thermal diffusivity of the foam is estimated by dividing the expression for the thermal conductivity above by the heat capacity of polycarbosilane at the onset of curing (1600 $\mathrm{J\,kg^{-1}\,^\circ C^{-1}}$ at 125 °C[18]), as well as the density of the polycarbosilane foam, which is simply the density of the solid polycarbosilane (1.2 $\mathrm{g\,cm^{-3}}$) multiplied by V_f. Hence, $k/\rho C_p = 9.30 \times 10^{-8}\ \mathrm{m^2\,s^{-1}}$.

3.2.2. Heat transfer coefficient

For forced convection around macroscopic cylinders the correlation of Churchill and Bernstein is used [19]

$$\mathrm{Nu_f} = 0.3 + \frac{0.62\ \mathrm{Re}^{1/2}\mathrm{Pr}^{1/3}}{[1 + (0.4/\mathrm{Pr})^{2/3}]^{1/4}}\left[1 + \left(\frac{\mathrm{Re}}{282\,000}\right)^{5/8}\right]^{4/5} \quad (5)$$

where Re is the Reynolds number $= Du\rho'/\mu$, Pr the Prandtl number $= C'_p\mu/k'$, Nu the Nusselt number $= hD/k'$, D the cylinder diameter, u the air velocity, ρ' the density of air, μ the viscosity of air, C'_p the heat capacity of air, k' the thermal conductivity of air, and h the heat transfer coefficient. The upper limit of this equation appears to be in excess of $\mathrm{Re} = 10^7$. The lower limit occurs at about $\mathrm{RePr} < 0.2$ (roughly $\mathrm{Re} = 0.28$ for air) [19].

For natural convection around macroscopic cylinders, the correlation of Churchill and Chu is used [20]

$$\mathrm{Nu_n} = \left[0.60 + 0.387\left(\frac{\mathrm{GrPr}}{[1 + (0.559/\mathrm{Pr})^{9/16}]^{16/9}}\right)^{1/6}\right]^2 \quad (6)$$

where Gr is the Grashof number $= D^3\rho'^2 g\beta\Delta T/\mu^2$, g the acceleration due to gravity, β the coefficient of thermal expansion for air, and ΔT the temperature difference between cylinder and ambient. The upper limit of the correlation appears to be in excess of $\mathrm{Gr\,Pr} = 10^{12}$, while the lower limit occurs at roughly $\mathrm{Gr\,Pr} = 10^{-6}$ ($\mathrm{Gr} > 1.4 \times 10^{-6}$ for air) [20].

To compute the effective heat transfer coefficient based on the contributions of natural and forced convection, the following equation, suggested by Churchill [21], is used

$$\mathrm{Nu} = (\mathrm{Nu_f^3} + \mathrm{Nu_n^3})^{1/3} \quad (7)$$

The heat transfer coefficient measured by heating the copper cylinder was $h = 25.2\ \mathrm{Wm^{-2}K^{-1}}$. This value is equal to the value of the heat transfer coefficient predicted by Churchill's correlation (Equation 5) for air flowing over a cylinder 2 cm in diameter at a velocity of 1.18 $\mathrm{m\,s^{-1}}$ (for a temperature of 150 °C); this value for u is used in the computer model.

3.3. Failure criteria

Polycarbosilane foam can fail in two ways during curing, either by cracking or by melting. Melting occurs if the temperature is raised so quickly that the polycarbosilane does not have time to cross-link before elevated temperatures are reached. The temperature at the onset of melting (for PC-470), as a function of weight gain has been studied by Ichikawa *et al.*, and is described elsewhere [22]. Experimentally, the weight gain of polycarbosilane foam cured from 100–190 °C at 0.02 $^\circ\mathrm{C\,min^{-1}}$ was found to be 10.1%. The amount of heat liberated during this cycle is 3600 $\mathrm{J\,g^{-1}}$, by integration of equations for curing kinetics from Part I. Assuming weight gain is proportional to the total heat evolved, polycarbosilane is calculated to liberate 357 $\mathrm{W\,g^{-1}}$ for every 1% in weight gain. The data of Ichikawa can then be redrawn as the temperature at the onset of melting, T_s, versus the total heat evolved, Q_{tot}, Fig. 9. The data were found to fit well to the following equation

$$T_s = 176 + 1.444 \times 10^{-5} \times Q_{tot} + 1.289 \times 10^{-11} Q_{tot}^2 \quad (8)$$

with Q_{tot} in $\mathrm{J\,kg^{-1}}$, plotted as a full line in Fig. 9 . Melting is thus predicted if the temperature of the sample exceeds $T_s(Q_{tot})$ anywhere.

Beyond a weight gain of 6.5% (which corresponds to 2320 $\mathrm{W\,g^{-1}}$), Ichikawa found PC-470 infusible. Beyond this critical degree of cross-linking polycarbosilane foam will therefore not melt, even when thermal runaway occurs. Rather, cracks are expected to form due to thermal stresses within the sample if high-temperature gradients are present.

Using the criterion just described, processing maps were constructed which predict under what conditions the curing of polycarbosilane foam will be stable. A computer program was designed to map the boundary between stable curing and thermal runaway (all computer codes are listed elsewhere [15]), using, as a criterion for thermal runaway, a core temperature exceeding 300 °C. A similar program was also developed to map process parameters which lead to melting of the sample by testing at each iteration whether the sample temperature exceeds T_s.

4. Discussion

A simple steady-state heat flow calculation, given in Appendix 4 of [15], shows that in monitored curing

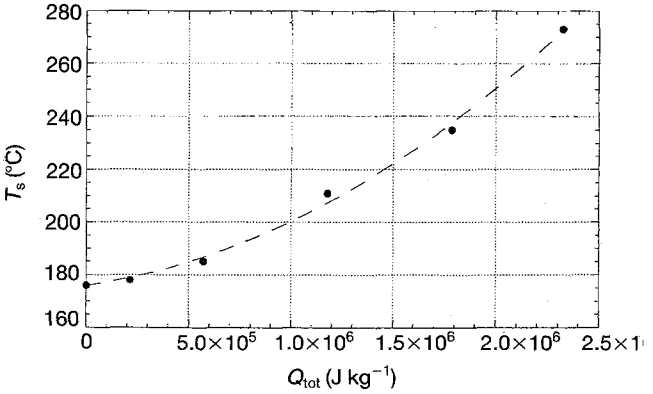

Figure 9 Predicted temperature at the onset of melting, T_s, as a function of the heat evolved during curing.

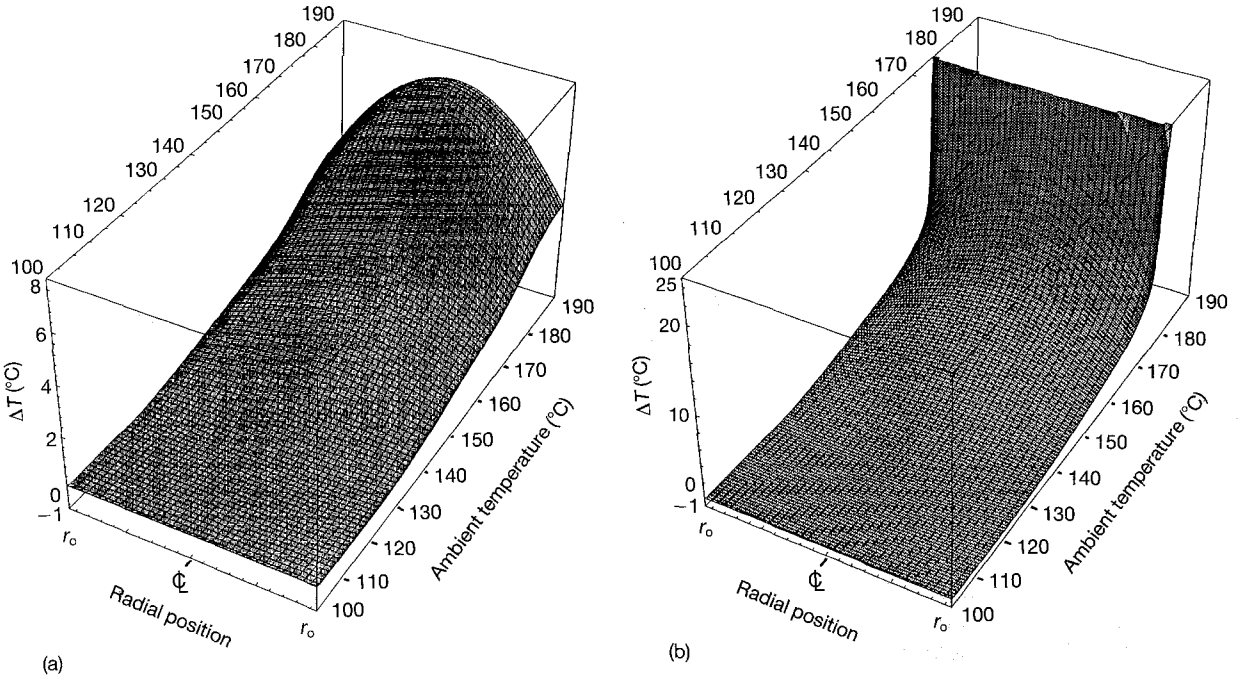

Figure 10 (a) Predicted curve of sample temperature as a function of time and radius plot for stable curing; (b) same for thermal runaway. For both samples the ambient temperature increase rate is 0.1 °C min^{-1}, the volume fraction polycarbosilane is 0.4 and the air velocity is 1.18 m s^{-1}, in (a) sample diameter is 0.76 cm, in (b) it is 1.27 cm.

experiments, the thermocouple measuring temperature inside the sample (shown in Fig. 4) provides a signal which is proportional to the actual temperature difference between the sample core and the surrounding atmosphere, but may underestimate very significantly this difference (due to heat transfer by conduction along its metal wire). The thermocouple measuring ambient temperature is, on the other hand, precise. Therefore, the experimental apparatus provides a measurement of the *ambient* temperature, T_{crit} (reported in Table II) at which thermal runaway or an exotherm peak occurs; however, the actual temperature inside the sample is not known.

Theoretical analysis of heat transfer within the samples was in qualitative agreement with experimental observations in that two types of thermal history were predicted. In some cases, predicted temperature profiles were such that sample core temperatures never exceeded the surrounding ambient temperature by more than a few degrees; an example is given in Fig. 10a. In other cases, thermal runaway was predicted, such that the sample core temperature would increase rapidly above the curing temperature range, producing steep temperature gradients across the sample diameter; and example is given in Fig. 10b. These features of thermal runaway, namely rapid heating to high temperatures and steep temperature gradients, explain the two sample failure modes observed, namely melting and cracking, respectively.

Quantitative agreement of theory with experiment was also good: a comparison of theoretical and experimental results for the six monitored curing runs A–F is shown in Table II. It is seen that the model correctly predicts system stability, as well as T_{crit} within 10 °C for every run.

Fig. 11 is a processing map corresponding to runs A–F ($u = 1.175$ m s^{-1}, $V_f = 0.40$). The results from

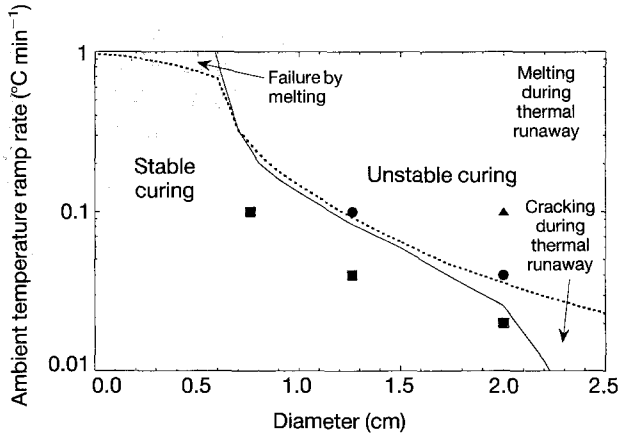

Figure 11 Processing parameter diagram mapping unstable and stable curing regimes for polycarbosilane foam. Air velocity is 1.175 m s^{-1}, PCS volume fraction is 0.4. Experimental points from Table II are superimposed on the diagram. (——) Thermal runaway border, (– – –) melting border, (■) successful samples, (●) cracked samples, (▲) melted sample.

runs A–F are superimposed on Fig. 11 to test the accuracy of the processing map. Samples A, D and F (which cured successfully) fall in the stable regime, as predicted. The dashed line in Fig. 11 maps the melting border. Samples B and E (which experienced thermal runaway, but showed no signs of melting) fall slightly above this line but are almost within the predicted cracking regime. Sample C (which experienced thermal runaway and displayed signs of melting) falls above this line, well within the melting regime.

Based on the good agreement between theory and experiment, the model was used to explore process parameter ranges and strategies for successful processing of the foams. It was found that system stability increases most dramatically with decreasing sample size, provided the ambient temperature is increased at

a rate below roughly 1 °C min^{-1}; otherwise, the model predicts that the polycarbosilane foam will melt or crack before reaching the end of the curing cycle. Figs 12 and 13 show the predicted effects of air velocity and relative density on the curing behaviour. Clearly, system stability increases with increasing air velocity and decreasing relative density; however, the effect of these parameters is not very strong: a ten-fold increase in the velocity, or a halving of V_f, only increase the maximum sample size by 25% at the same temperature ramping rate.

The processing maps therefore show that thermal management essentially restricts samples produced to geometries having at least one dimension below about 2 cm. The physical origins of this size restriction, namely (i) the relatively low thermal diffusivity of the polymer, (ii) the high heat released during conversion of the polymer, and (iii) the strong temperature dependence of the rate of oxidative curing, will exist in other materials systems and microcellular foam processes as well. Thermal management is therefore likely to be an important issue in many microcellular foam processes which rely on conversion of a polymer by chemical reaction, and it is possible that thermal effects contribute to the similar size restrictions that have been reported for microcellular carbon

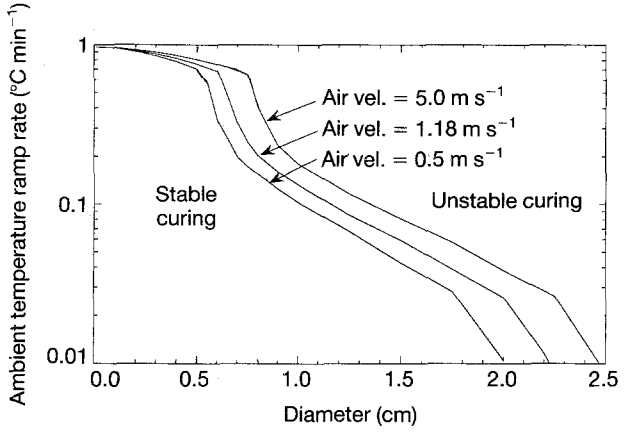

Figure 12 Processing parameter diagram mapping unstable and stable curing regimes for polycarbosilane foam for variable air velocity; PCS volume fraction is 0.4.

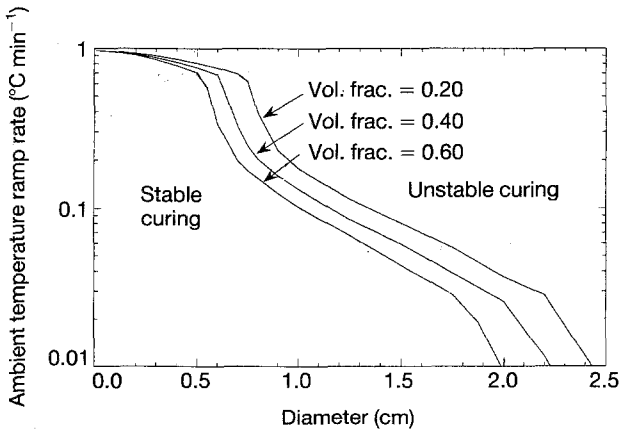

Figure 13 Processing parameter diagram mapping unstable and stable curing regimes for polycarbosilane foam for variable volume fraction PCS; air velocity is 1.175 m s^{-1}.

foams produced from polymer precursors in Table 1 of [3].

To increase the maximum sample size, alterations must be brought to the standard oxidative curing process used here. One option may be to control the rate of oxidative curing *via* control of the oxygen partial pressure; however, oxygen-free curing would be preferable, because it is known that oxygen introduced into polycarbosilane during curing subsequently reacts with the polycarbosilane during pyrolysis to form silica in the resulting SiC. This has been shown to reduce significantly its mechanical properties [23, 24]. At higher temperatures (1200–1400 °C) the effect of oxygen becomes increasingly severe: excess carbon in the SiC combines with SiO_2 to form CO which, in turn, creates voids within the ceramic, seriously degrading its mechanical properties [25, 26].

To improve the properties of polycarbosilane-derived SiC, alternative curing methods have been developed, including several irradiation techniques. When irradiated with electrons in a vacuum, polycarbosilane can be cross-linked without introducing oxygen. The resulting SiC fibres have been shown to have mechanical properties superior to those of fibres cured in oxygen [27–29]. Polycarbosilane can also be cured using γ-rays, in air (in the presence of air, Si–O–Si linkages similar to those formed during oxidative curing are formed, however), and in vacuum [29, 30]. Polycarbosilane has also been cross-linked by other methods, including exposure to ozone [31], chlorine and hydrogen peroxide [32]. Preceramic polymers other than polycarbosilane have similarly been cured using alternative techniques, including plasma treatment, exposure to ultraviolet radiation and electron-beam energy [33–36].

Curing methods other than the customary oxidative curing may therefore provide greater thermal control during curing, allowing in turn an increase in the maximum foam size produced by this process while, in some cases, improving the foam mechanical strength. In particular, radiation capable of penetrating the foam to sufficient depth provides an attractive alternative to oxidative curing, because it would allow independent control of the rate of heat extraction and the rate of cross-linking: the curing kinetics could then be controlled by controlling the radiation flux, while the initial foam temperature and surrounding fluid can be tailored for improved cooling.

5. Conclusion

A method for producing ceramic foams from preceramic polymer precursors is demonstrated using polycarbosilane as a precursor for silicon carbide. In this process, polycarbosilane is first pressure infiltrated into a porous sodium chloride compact, having a controlled particle size and density. The salt is subsequently leached away, the resulting polycarbosilane foam is cured by heating in air, and finally pyrolysed into a ceramic. Homogeneous open-celled silicon carbide foams were produced in this way, having controlled cell sizes varying roughly between 10 and 100 μm and controlled relative densities.

Analysis of heat transfer during oxidative curing in air of the foams was shown to agree with experimental data, proving that internal heat generation during curing may cause thermal runaway and degrade the foams produced in this process. Although alterations in process parameters may lead to marginal improvements, analysis shows that this phenomenon essentially restricts samples produced by this to a thickness of about 2 cm. To increase sample size, alternative curing methods, including deep-penetration irradiation processes, and curing with reduced oxygen partial pressure, which allow independent control of curing kinetics and rate of sample cooling, should be explored.

Acknowledgements

This work was sponsored by the Consortium for Inorganic Composites at MIT, and by a Kurtz Fellowship to T. Fitzgerald at MIT during the Fall of 1992.

References

1. T. J. FITZGERALD and A. MORTENSEN, *J. Mater. Sci.* **29** (1994) in press.
2. L. GIBSON and M. F. ASHBY, "Cellular Solids–Structure and Properties" Pergamon Press, Oxford, 1988) pp 1–357.
3. J. M. WILLIAMS and D. A. WROBLESKI, *J. Mater. Sci.* **24** (1989) 4062.
4. J. D. LEMAY, R. W. HOPPER , L. W. HRUBESH and R. W. PEKALA. *Mater. Res. Soc. Bull.* **15** (1990) 19.
5. A. J. SHERMAN, R. H TUFFIAS and R. KAPLAN, *Ceram. Bull.* **70** (1991) 1025.
6. D. B. LEISER, M. SMITH and D. A. STEWART, *Ceram. Eng. Sci. Proc.* **6** (1985) 757.
7. R. W. PEKALA and R. W. HOPPER, *J. Mater. Sci.* **22** (1987) 1840.
8. R. W. HOPPER and R. W. PEKALA, US Pat. 4806 290 (1989)
9. *Idem*, US Pat. 4756 898 (1988)
10. R. E. FISHER, C. V. BURKLAND and W. E. BUSTAMANTE, *Ceram. Eng. Sci. Proc.* **6** (1985) 806.
11. J. A. ISAACS, F. TARICCO, V. J. MICHAUD and A. MORTENSEN, *Metall. Trans.* **22A** (1991) 2855.
12. M. BERG, PhD thesis, Massachusetts Institute of Technology (1953).
13. F. B. SWINKELS and M. F. ASHBY, *Acta Metall.* **29** (1981) 259.
14. J. CRANK, "The Mathematics of Diffusion", 2nd Edn, (Oxford University Press, New York, 1975).
15. T. FITZGERALD, PhD thesis, 1993, Massachusetts Institute of Technology, June 1993.
16. H. ICHIKAWA, Nippon Carbon, private communication (1991).
17. M. A. SCHUETZ and L. R. GLICKSMAN, *J. Cell. Plastics* **20** (1984) 114.
18. H. SUWARDIE, MSc thesis, Stephens Institute of Technology (1988)
19. S. W. CHURCHILL and M. BERNSTEIN, *Trans. ASME J. Heat Transfer* **99** (1977) 300.
20. S. W. CHURCHILL and H. H. S. CHU, *Int J. Heat Mass Transfer* **18** (1975) 1049.
21. S. W. CHURCHILL, *AIChE J.* **23** (1977) 10.
22. H. ICHIKAWA, F. MACHINO, H. TERANISHI and T. ISHIKAWA, "*Advances in Chemistry Series*", edited by J. M. Zeigler and F. W. G. Fearon (American Chemical Society, Washington, DC 1990) pp. 619–37.
23. K. OKAMURA, M. SATO and Y. HASEGAWA, *J. Mater. Sci. Lett.* **2** (1983) pp. 769–771.
24. H. ICHIKAWA, H. TERANISHI and T. ISHIKAWA, *ibid.*, **6** (1987) 420.
25. K. OKAMURA, M. SATO and T. MATSUZAWA, *Ceram. Eng. Sci. Proc.* **9** (1988) 909.
26. G. S. BIBBO, P. M. BENSON and C. G. PANTANO, *J. Mater. Sci.*, **26** (1991) 5075.
27. K. OKAMURA, M. SATO and Y. HASEGAWA, *Ceram. Int.* **13** (1987) 55.
28. T. TAKI, K. OKAMURA, M. SATO, T. SEGUCHI and S. KAWANISHI *J. Mater. Sci. Lett.* **7** (1988) 209.
29. K. OKAMURA, H. SATO, T. SEGUCHI and S. KAWANISHI in "*Proceedings of the Ist Japan International SAMPE Symposium*" (1989) pp. 929–34.
30. K. OKAMURA, T. MATSUZAWA and Y. HASEGAWA, *J. Mater. Sci. Lett.* **4** (1985) 55.
31. K. J. WYNNE and R. W. RICE, *Ann. Rev. Mater. Sci.* **14** (1984) 297.
32. S. YAJIMA, J. HAYASHI and M. OMORI, US Pat. 4100 233 (1978).
33. J. LIPOWITZ, US Pat. 4743 662 (1988).
34. M. A. LUTZ, R. S. REAOCH and P. R. REEDY, US Pat. 4816 497 (1989).
35. J. M. SCHWARK, US Pat. 5021 533 (1991).
36. *Idem*, US Pat. 5155 181 (1992).

Received 30 September 1993
and accepted 9 June 1994